Springer

Journal of
Mechanical
Science and
Technology

Journal of Mechanical Science and Technology 22 (2008) 50~60

www.springerlink.com/content/1738-494x

Dynamic analysis of a linear motion guide having rolling elements for precision positioning devices

Yong-Sub Yi[1], Yoon Young Kim[1,*], Jae Seok Choi[2], Jeonghoon Yoo[2], Dong Jin Lee[3], Suk Won Lee[3] and Sung Jin Lee[3]

[1]*National Creative Initiatives Center for Multiscale Design, School of Mechanical and Aerospace Engineering, Seoul National University, San 56-1 Shinlim-Dong, Kwanak-Gu, Seoul 151-742, Korea*

[2]*Department of Mechanical Engineering, Yonsei University,134 Shinchon-Dong, Seodaemun-Gu, Seoul 120-749, Korea*

[3]*Mechatronics Center, Samsung Electronics Co., Ltd.,416 Maetan 3-Dong, Yeongtong-Gu, Suwon-Si, Gyeonggi-Do 443-742, Korea*

(Manuscript Received October 9, 2006; Revised June 15, 2007; Accepted July 12, 2007)

Abstract

Linear motion (LM) guides supported by rolling elements can be used to ultra-accurately position precision machines. For accurate positioning, the micro and macro dynamic behavior of the LM guide must be understood, but the research on this subject is rather limited. In this investigation, experiments to reveal the dynamic characteristics of the LM guide were performed and a simplified model to predict the observed dynamics of the LM guide was developed. Several experiments conducted in the present research demonstrated the hysteretic behavior as well as frequency- and force-dependent phenomena of the LM guide. The validity of the proposed modeling method was checked with theoretical and numerical analyses.

Keywords: Linear Motion (LM) guide; Micro-friction model; Contact analysis; Dynamic analysis

1. Introduction

Linear motion (LM) guides have been widely used for ultra-precise positioning devices to transport machine parts through a linear path in machining centers and X-Y tables etc. With machine parts becoming smaller and finer, the required order of precision has increased. This research presents some experimental results on ball bearing-supported LM guides up to micro-scale level and develops techniques to predict the dynamic characteristics of LM guides, such as their eigenfrequencies.

Compared to LM guides supported by non-contact bearings such as air bearings requiring complex and expensive fabrication processes [1], LM guides using ball bearings have advantages such as high stiffness, relatively good reliability, and low cost. However, nonlinear dynamic behavior of ball bearings needs to be considered for accurate prediction of the motion of LM guides.

The dynamic characteristics of the LM guide can be largely classified into elastic deformation-induced dynamics and friction-induced dynamics. The friction-induced dynamics will be referred to as the dynamics of the LM guide in the moving direction, while the elastic deformation-induced dynamics as that in other directions.

For the friction-induced dynamics, some investigations have employed micro-scale friction models. Micro-scale friction models can simulate nonlinear characteristics that cannot be described by classical friction models using the Coulomb friction, the Stribeck effect and the others. Since the dynamic model describing spring-like behavior in stiction state (static friction) proposed by Dahl [2], several modi-

*Corresponding author. Tel.: +82 2 880 7154, Fax.: +82 2 872 5431
E-mail address: yykim@snu.ac.kr
DOI 10.1007/s12206-007-1006-9

fied models [3-7] have been proposed. Most of the previous researches have investigated the rotor-arm system [8, 9], but only few researches have applied the micro-friction model to control the linear motor-driven LM guide system [10]. Though a practical control issue was considered in their work, the friction-induced dynamics of the LM guide has not been fully investigated.

Ohta [11] and Ohta and Hayashi [12] performed linear vibration analysis for the elastic deformation-induced dynamics. They carried out modal tests for a ball bearing-supported LM guide system which moved at a constant speed and determined the natural frequencies and the corresponding mode shapes including rigid-body modes and some flexural modes. Then they carried out simulations analytically and numerically. The eigenfrequencies of the LM guide system for five fundamental modes (excluding the motion related to the degree of freedom in the moving direction) were well predicted by their approach. Mekid [13] also carried out finite element analysis of the hydrostatic bearing-supported LM guide system. The above-mentioned research has contributed substantially to the understanding of the LM guide system dynamics, but their modeling techniques are not fully based on theoretical analyses.

Our study consists of two parts: the presentation of the experimental results for the ball bearing-supported LM guide, and the theoretical modeling technique of the bearing ball stiffness for elastic deformation-induced dynamic analysis. For the theoretical modeling, we newly developed a technique based on the Hertz contact analysis of ball bearing to evaluate equivalent stiffness and predicted some natural modes and frequencies by establishing an adequate finite element model. Also, the development of a complete theoretical model to predict friction-induced dynamics of the LM guide by the LuGre model [3] was tried; however, it was not successful. Nevertheless, the experiments showed the interesting nonlinear phenomena that occurred when the system moved very slowly.

2. Dynamic behavior of LM guide

To study the LM guide dynamics experimentally, modal tests were conducted first. The LM guide used in this study was manufactured by THK Co. Ltd. It transports an LM block by use of 4 rows of recirculating balls, as shown in Fig. 1. Between balls, cages are located to prevent balls from interacting.

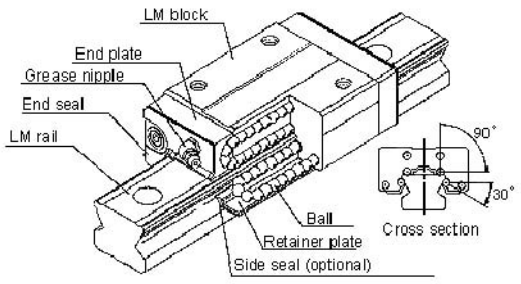

Fig. 1. Schematic of the LM (Linear Motion) guide.

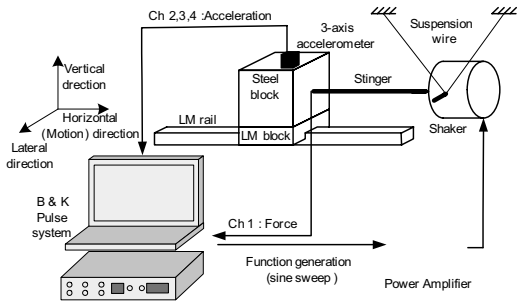

Fig. 2. The experimental setup.

Table 1. Experimental results for natural frequencies (Hz).

Mode No.	Axial excitation	Lateral excitation	Vertical excitation
1st	0~74		
2nd	158	153	149
3rd	422	416	422
4th	487	497	467
5th			1190
6th	1460	1450	1590

The LM guide assembly including the block carrying the payload is shown in Fig. 2. The steel block was excited by a modal shaker in the three directions: horizontal, lateral and vertical. The horizontal direction was the LM guide's direction of motion. A tri-axis accelerometer was located at the corners of the steel block. Fig. 2 shows the schematic setup of the modal testing. The excitation frequency was varied from 0 Hz to 3.2 kHz at the sweeping rate of 5 Hz/sec. The excitation force level was also varied between 0.1 N and 5 N.

Table 1 shows the eigenfrequencies of the LM guide system, which were extracted from the measured frequency response functions shown in Fig. 3. Fig. 4 shows the mode shapes of the steel block that correspond to the eigenfrequencies listed in Table 1. Four to six eigenfrequencies exist in each excitation direction. To characterize the mode shapes, each mode shape is referred to as the (horizontally-)translational, rolling, yawing, pitching, or bouncing and high-order rolling mode. Five modes from rolling to high-order rolling modes were also observed in earlier researches [11, 12]. The flexural modes caused by the elastic deformation of the LM block or the LM rail were not present in the frequency range concerned, for they have relatively higher natural frequencies than the rigid body modes.

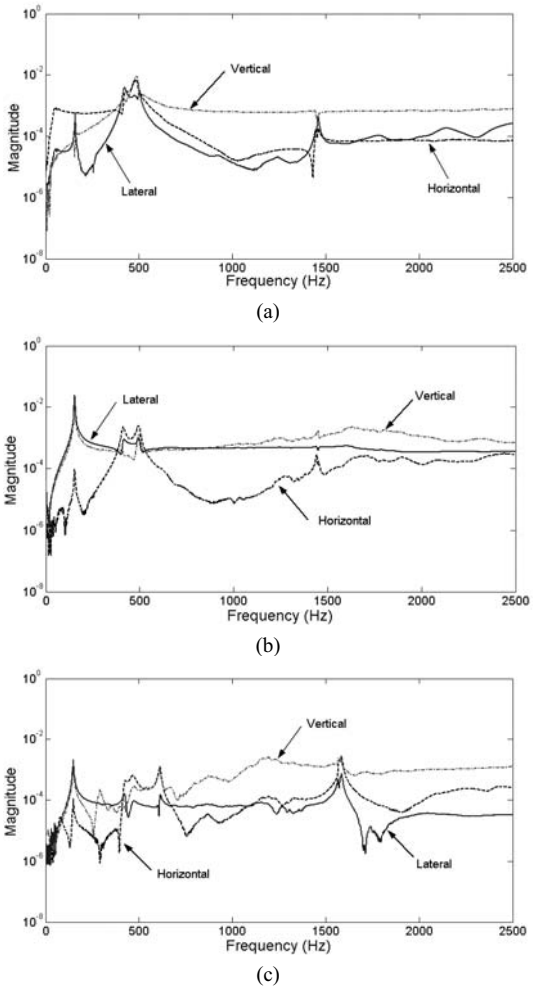

Fig. 3. Typical frequency responses obtained by excitations in the (a) horizontal, (b) lateral and (c) vertical directions.

Except the first eigenmode (i.e., the horizontally-translational mode), the mechanics behind the every rigid body modes is somewhat obvious; the elastic deformations of the bearing balls which lay between the LM block and the LM rail were responsible for the 2nd to 6th vibration modes. At a glance, however, the mechanism generating the first mode was not clear. Its eigenfrequency considerably varied depending on the experimental conditions, such as the magnitude of the excitation force. Earlier investigations [14, 15] reported the nonlinear behavior related to the first mode, but the physics behind it has not been fully explained.

3. Elastic deformation-induced dynamics

In this section, the theoretical analysis to predict the

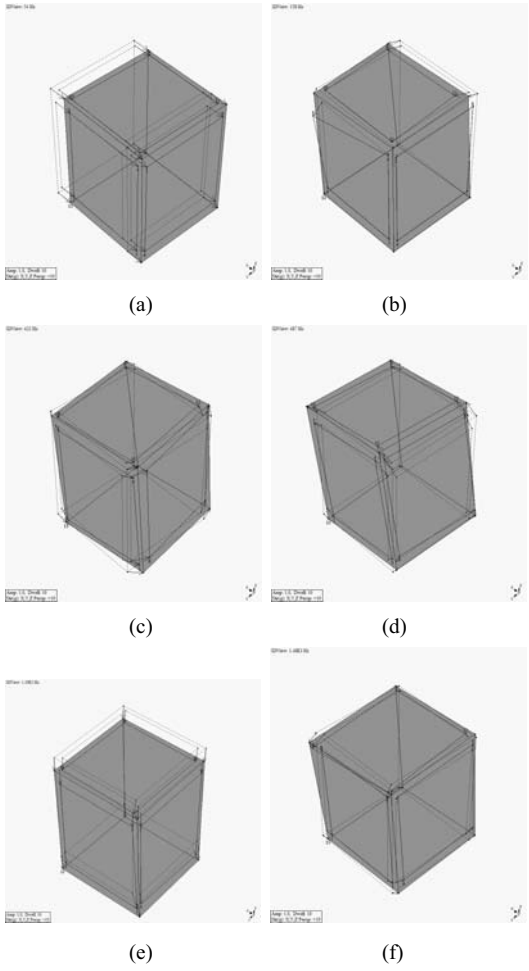

Fig. 4. Mode shapes: (a) translation, (b) rolling, (c) yawing, (d) pitching, (e) bouncing and (f) high-order rolling.

2nd up to the 6th eigenfrequencies and eigenmodes, which are associated with the elastic deformation of the LM block, LM rail and bearing balls, will be presented. The key procedure in this analysis is the estimation of the equivalent stiffness and effective modeling of the LM guide system. For these two tasks, contact analysis was carried out. Though some earlier investigations used the contact mechanics approach for the LM guide systems, they, however, were mainly concerned with fatigue analysis and lifetime estimate [16].

3.1 Evaluation of equivalent stiffness

The Hertz contact model is most widely used for contact analysis. However, it needs the solution of complicated integral equations. To facilitate analysis, a simplified model based on the elastic foundation concept [17] is used in this investigation.

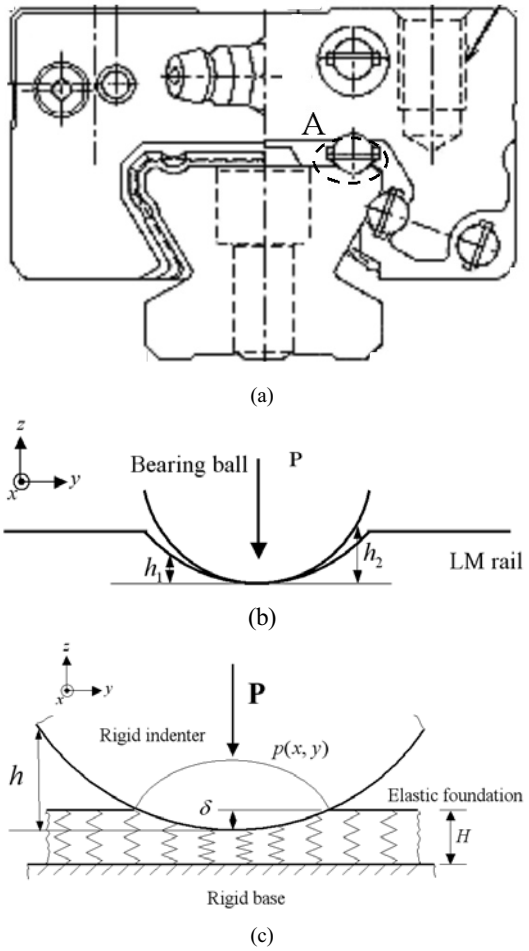

Fig. 5. (a) Section view of the LM block and the rail, (b) enlarged diagram of part A and (c) schematic diagram of the elastic foundation model.

The contact plane between a bearing ball and the LM rail, which is shown in part A in Fig. 5(a), is replaced by the elastic foundation of height, H, which rests on a rigid base, and is compressed by a rigid indenter as in Fig. 5(c). The profile of the indenter $h(x,y)$ is taken as the sum of the profiles of the contacting two bodies – $h_1(x,y)$ of the LM rail and $h_2(x,y)$ of the bearing ball as shown in Fig. 5(b), i.e.,

$$h(x,y) = h_1(x,y) + h_2(x,y)\,. \tag{1}$$

If the curved profile of the indenter is assumed to be continuous up to its second derivative in the contact region, the profile may be written as:

$$h(x,y) = \frac{1}{2R'}x^2 + \frac{1}{2R''}y^2 \tag{2}$$

where R' and R'' are the relative principal radii of curvature at the origin.

If the penetration by the applied force P at the origin is denoted by δ, then the normal elastic displacement component field of the foundation u_z is given by

$$u_z(x,y) = \begin{cases} \delta - h(x,y) & \delta > h \\ 0 & \delta \le h \end{cases} \tag{3}$$

Since the contact pressure at any point depends only on the displacement at the point, one can write

$$p(x,y) = \frac{K}{H}u_z(x,y) \tag{4}$$

where K is the elastic modulus of the foundation and will be given later.

Using Eqs. (2)~ (4), the pressure $p(x,y)$ inside the contact area can be written as

$$p(x,y) = \frac{K\delta}{H}\left(1 - \frac{x^2}{a^2} - \frac{y^2}{b^2}\right) \tag{5}$$

where $a = \sqrt{2\delta R'}$ and $b = \sqrt{2\delta R''}$ denote the semi-axes of the ellipsoidal contact area.

The integration of the pressure in Eq. (5) over the

contact area yields the total load, which is

$$P = \frac{K\pi ab\delta}{2H} \tag{6}$$

It is well known that $\frac{K}{H} = 0.60\frac{E^*}{r}$ should be used for the case of axisymmetric contact [17] where r is the contact radius and E^* is given by $\frac{1}{E^*} = \frac{1-\nu_1^2}{E_1} + \frac{1-\nu_2^2}{E_2}$ (E : Young's modulus, ν : Poisson's ratio). Thus, one may replace r with the equivalent radius $(ab)^{\frac{1}{2}} = \left(\sqrt{2\delta R'}\sqrt{2\delta R''}\right)^{\frac{1}{2}} =$, $\sqrt{2}\left(R'R''\right)^{\frac{1}{4}}\delta^{\frac{1}{2}}$ and the following load-penetration relation is obtained:

$$P = \frac{0.60E^*\pi\left(R'R''\right)^{\frac{1}{4}}}{\sqrt{2}}\delta^{\frac{3}{2}} = C\delta^{\frac{3}{2}}. \tag{7}$$

By representing the groove radius of the LM rail by r_1 and the ball radius by r_2, the rail profile h_1 and the ball profile h_2 can be written as

$$h_1 = \frac{1}{2R_1'}x^2 + \frac{1}{2R_1''}y^2 = -\frac{1}{2\times\infty}x^2 - \frac{1}{2r_1}y^2 = -\frac{1}{2r_1}y^2 \tag{8}$$

$$h_2 = \frac{1}{2R_2'}x^2 + \frac{1}{2R_2''}y^2 = \frac{1}{2r_2}x^2 + \frac{1}{2r_2}y^2. \tag{9}$$

Substituting Eqs. (8) and (9) into Eq. (1) yields the profile h of the rigid indenter:

$$h = h_1 + h_2 = \frac{1}{2r_2}x^2 + \left(\frac{1}{2r_2} - \frac{1}{2r_1}\right)y^2 = \frac{1}{2R'}x^2 + \frac{1}{2R''}y^2 \tag{10}$$

Therefore, the relative principal radii of the rigid indenter may be identified as

$$R' = r_2 \quad R'' = \frac{1}{\frac{1}{r_2} - \frac{1}{r_1}} = \frac{r_1 r_2}{r_1 - r_2} \tag{11}$$

Differentiating Eq. (7) with respect to δ yields the equivalent stiffness k due to the elastic deformations of the bearing ball and the rail:

$$k = \frac{dP}{d\delta} = \frac{3}{2}\left(\frac{\pi\left(0.60E^*\right)}{\sqrt{2}}\left(R'R''\right)^{1/4}\right)\delta^{\frac{1}{2}} \equiv \frac{3}{2}C\delta^{\frac{1}{2}} \tag{12}$$

Since E^* is the material property and R' and R'' are geometrical data, one can see from Eq. (12) that the equivalent stiffness varies only with $\delta^{\frac{1}{2}}$. Therefore, the stiffness of the LM guide can be controlled by the preload, which is caused by the negative clearance of the bearing balls.

3.2 Analysis results

Eq. (12) is used to compute the stiffness of a linear spring in the analytic solution and finite element analysis of the LM guide system, and these analyses check the validity of our proposition in explaining correctly the modal behavior of the system from the 2nd to the 6th eigenmode shown in Table 1 and Fig. 4.

In earlier works, the lowest five natural frequencies were obtained analytically as follows (for details, see Appendix).

$$f_{bouncing} = \frac{1}{2\pi}\sqrt{\frac{2L(K_1 + K_2\sin^2\beta)}{M}} \tag{13}$$

$$f_{pitching} = \frac{1}{2\pi}\sqrt{\frac{L^3(K_1 + K_2\sin^2\beta)}{6J_y}} \tag{14}$$

$$f_{yawing} = \frac{1}{2\pi}\sqrt{\frac{K_2L^3\cos^2\beta}{6J_Z}} \tag{15}$$

$$\begin{cases} f_{rolling} = \omega_1/2\pi \\ f_{high-rolling} = \omega_2/2\pi \end{cases} \tag{16}$$

In Eq. (16) ω_1 and ω_2 satisfy the following equation:

$$Det\left(\begin{bmatrix} p_1 - M\omega^2 & p_2 \\ p_2 & p_3 - J_x\omega^2 \end{bmatrix}\right) = 0 \tag{17}$$

$$\begin{aligned} p_1 &= 2K_2L\cos^2\beta \\ p_2 &= K_2L(2b\cos^2\beta - c_2\sin 2\beta) \\ p_3 &= 2L(K_1c_1^2 + K_2b^2\cos^2\beta + K_2c_2^2\sin^2\beta - K_2bc_2\sin 2\beta) \end{aligned} \tag{18}$$

In preceding equations K_1 and K_2 denote the equivalent stiffnesses of the upper and lower row of the bearing balls, M the total mass of LM block and steel block, J_x, J_y and J_z the moment of inertia of the LM block and steel block about the *x*-, *y*- and *z*-axes, respectively. The *x*-axis corresponds to the motion direction and the *y*- and *z*-axes correspond to the lateral and vertical direction, respectively, and they have the origin at the mass center. What L, b, c_1, c_2 and β represent is shown in Fig. 6.

Two analysis models are used for finite element calculation. One model treats the LM block and the steel block as a rigid body while the other, as solid brick elements. For the rigid body modeling, a concentrated mass is placed at the mass center with an equivalent moment of inertia, and then a rigid body is constructed by linking the springs and the mass center with massless rigid beams. For the solid brick element modeling, 8-node brick elements are used, which were meshed by the Altair HyperMesh software. The bearing balls are replaced by equivalent linear spring elements, and therefore, 14 spring elements are located at each row, respectively. For modal analysis, the block Lanczos method of the ANSYS 7.0 is used.

To model the prestress effect by the negative toler

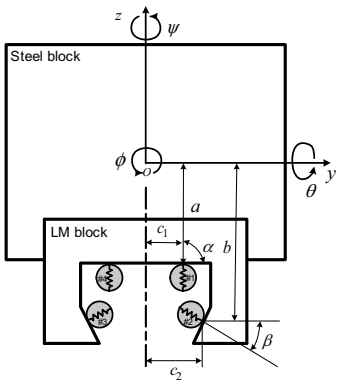

Fig. 6. Geometry of the LM guide system.

ance between the balls and the rail, each of the spring elements is compressed by an initial displacement of 7 μm. This value is the mean value of the negative tolerance estimate given by the manufacturer, THK Co. Ltd., which ranges from 4 μm to 10 μm. Though it was not possible to measure the exact tolerance value, the validity of using it was checked indirectly by the experiments conducted by Choi et al. [18]. Analysis results for natural frequencies are presented in Figs. 7, 8 and Table 2. Analytical and FEM-based numerical results showed good agreement. Especially, the analytic solution and the FEM results with rigid body modeling showed very similar results. Note that the same concentrated mass and the moment of inertia are used and the LM block is treated as a rigid body for both methods. Because the flexural modes of the LM block and the steel block are much higher than the frequency range of concern, that is, their stiffness are much higher than those of the bearing balls, treating the blocks as rigid bodies is reasonable.

The predicted eigenfrequencies by the analytic and numerical solution are somewhat different from the experimental eigenfrequencies for higher modes. This might be because very simple one-dimensional equivalent stiffness was used and the nonlinearity shown in contact analysis was not applied. Considering that the modal orders and mode shapes well agree with the experimental results and the errors for lower modes are less than 15%, however, the results appear quite satisfactory.

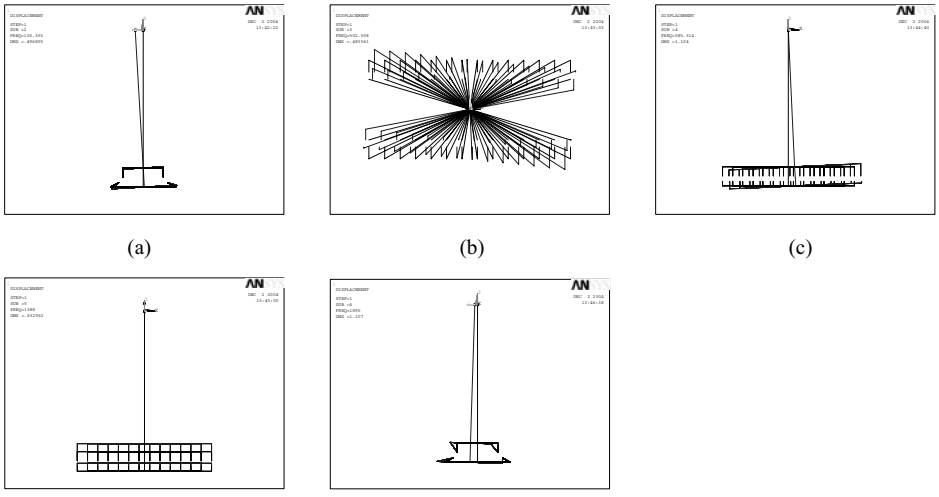

(a) (b) (c)

(d) (e)

Fig. 7. Mode shapes obtained by FEM analysis using rigid elements: (a) rolling, (b) yawing, (c) pitching, (d) bouncing and (e) high-order rolling.

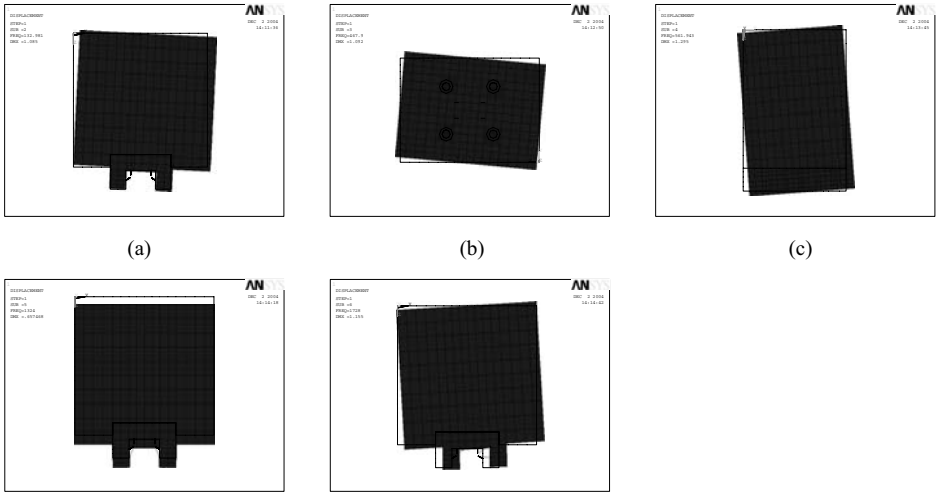

Fig. 8. Mode shapes obtained by FEM analysis using solid elements: (a) rolling, (b) yawing, (c) pitching, (d) bouncing and (e) high-order rolling.

Table 2. Analysis results by the Euler-Lagrange equation and the finite element method (FEM I: rigid modeling, FEM II: solid modeling).

Mode shape	Experiment	Theory	FEM I	FEM II
Rolling	153	137.3	136.3	133.0
Yawing	422	468.4	502.5	467.9
Pitching	487	545.3	585.3	561.9
Bouncing	1190	1389	1388	1324
High rolling	1450	1889	1890	1728

4. Friction-induced dynamics

4.1 Hysteresis test

To understand the type of nonlinearity involved in the first eigenmode, a number of experiments were conducted in which the excitation force was varied from 0.2 N to 4.2 N. The steel block was excited in the horizontal direction and the displacement of a point in the block was measured by the laser Doppler vibrometer (LDV). In the present experiments, a very low excitation frequency (under 1 Hz) was selected to minimize the inertial effect of the block and effectively show the static relationship between the excitation.

These experiments gave the following findings. When the excitation force exceeded approximately 4.2 N, which was the maximum static friction force, the balls rolled, as shown in Fig. 9(d). Even when the applied force is apparently smaller than the maximum static friction force, quite significant hysteretic motions are observed. From the viewpoint of classical friction, there should be no motion, that is, there should be no stiffness for the motion.

The mechanics behind these phenomena is not fully understood, but the micro-scale elastic and plastic deformations of the balls and the contacting regions caused by friction are likely to be responsible for the hysteretic force-displacement relation. Earlier researches reported similar phenomena between two sliding plates or in the rotor-bearing system. However, these researches considered quasi-static characteristics more important than dynamic characteristics.

The mean slope of the hysteresis loop in Figs. 9(a)-(c) could be regarded as the linear stiffness. As the excitation force increases, the mean slope decreases and the inside area of the loop increases. This means that the apparent system stiffness decreases and the dissipated energy increases as the force increases. This dependency on the excitation force level causes nonlinearity such as variable natural frequency for the first translational mode.

The effect of the excitation frequency is shown in Fig. 10. The excitation force level is fixed, and then the system response is observed for various excitation frequencies. When the excitation frequency is below 20 Hz, the overall loop pattern is similar to that obtained in the earlier results shown in Figs. 9(a)-(c). If we presume that the equivalent stiffness of the system

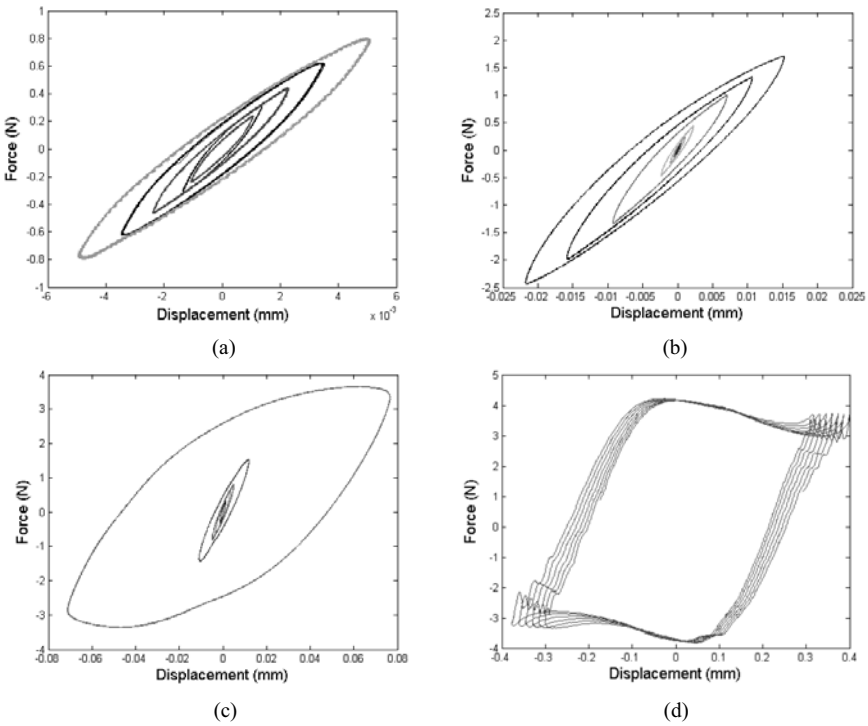

Fig. 9. Force-displacement relation for various force levels (a), (b), (c) before rolling and (d) after rolling.

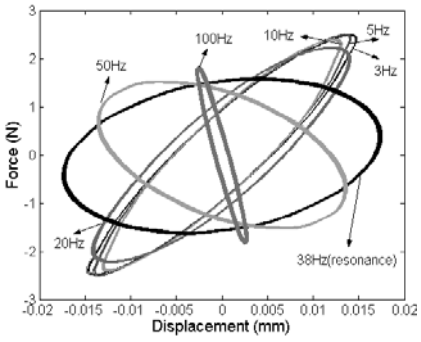

Fig. 10. Force-displacement relation curve at various excitation frequencies.

as the average slope of the quasi-static experimental results at low frequency and predict the natural frequency of the system by using a simple one-degree-of-freedom model, we can obtain 41.5 Hz from $f = \frac{1}{2\pi}\sqrt{\frac{k}{m}}$ for system mass m=2.50 kg. This frequency is very close to the experimental result of 38 Hz. When the excitation frequency approaches to the resonance frequency, the mean slope becomes almost zero. For higher-frequency excitations, the sign of the mean slope becomes negative. Since the one-degree-of-freedom mass-spring-damper system exhibits similar behavior, one may attempt to explain the phenomena by an equivalent one-degree-of-freedom model [14, 15].

4.2 Micro-friction model

In our investigation, the simulation of the phenomena observed in Figs. 9 and 10 is tried through the LuGre model [3], which is a popular modern friction model. Even though other models such as the Leuven model [4, 7] and the elastoplastic model [5] are available, they are equivalent to the LuGre model if the reverse point is fixed. In the LuGre model, pre-rolling displacement occurs due to the deformation of a large number of bristles at the contact surface. So, the motion is described by average bristle displacement as follows:

$$F = \sigma_0 z + \sigma_1 \dot{z} + \sigma_2 \dot{x} \tag{19}$$

$$\dot{z} = \dot{x} - \frac{|\dot{x}|}{g(\dot{x})} z = f(\dot{x}, z) \tag{20}$$

The symbols used in Eqs. (19) and (20) represent:
F : is the friction force;
z : the average bristle deflection;

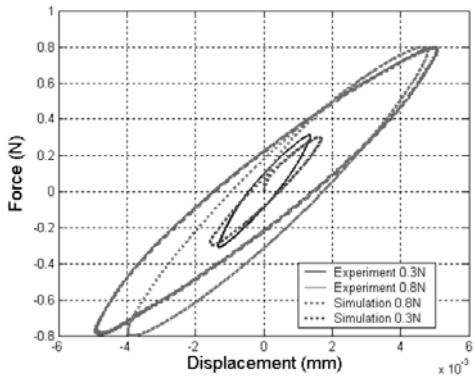

Fig. 11. Simulation results by using the LuGre model.

x : the relative displacement between the two contacting surfaces;

$g(\dot{x})$: the Stribeck curve for steady-state velocities;

σ_0 : the bristle stiffness;

σ_1 : the bristle damping;

σ_2 : the viscous damping coefficient.

The values of σ_0, σ_1 and σ_2 cannot be known before an experiment is carried out. Therefore, their values were determined by the least-square method [19] which was applied to the test results obtained at the excitation force of 0.5 N. Then other cases were simulated by using Eq. (19) and (20). As may be seen in Fig. 11, the model coefficients matching experimental results obtained for a specific condition (force level and frequency) may not simulate the experimental results obtained for other conditions. This is because the LuGre model has some defect in which the stiffness at the reverse point is invariable regardless of the position or velocity of the block [8]. Though some reports [3-7] have stated that the trajectory of the block is always the same from the point at which the direction of motion reverses, our experiments show that each trajectory of the block moves along different paths as the excitation force changes. Perhaps, an improved model considering up to the physics not covered by the LuGre model such as rigid body rolling should be developed, and the development of such a model will be pursued in future investigations.

5. Conclusion

We have investigated the dynamic properties of the LM guide system, both experimentally and theoretically. The natural frequencies of the system and the corresponding mode shapes have been observed through modal tests. In addition, hysteresis, which results from micro-scale friction in slowly moving LM guide systems, was investigated. The nonlinearity of the first translation mode was identified to result from the hysteresis. The force-displacement relation observed on the contact surface of the bearing balls and the rail of LM guide was derived by using the elastic foundation contact model, and the equivalent stiffness was also obtained from contact analysis. This relation was used for the dynamic analysis of the LM guide system except for the first natural mode, a translational mode. The dynamic analysis was conducted analytically and numerically. For the analytical solution, the Lagrange equation was used, and for the numerical solution, the finite element method modeling the LM block and the steel block as a rigid body and the bearing balls as linear spring elements was used. The analytical and numerical solutions agreed fairly well with the experimental results within about 15% error. To simulate the first eigenmode related to the hysteresis phenomenon, a micro-scale friction model based on the LuGre theory was adopted. Although the LuGre model was capable of capturing the main physical phenomena, it should be improved to accurately describe the experimentally observed phenomena. The contact analysis based on the dynamic model developed in this investigation can be a useful initial tool for the LM guide system design. However, the ultra-precise control of the system requires an advanced hysteresis analysis model, which can be a good research subject in the future.

Acknowledgments

This study was supported by the Mechatronics Center of SAMSUNG Electronics.

References

[1] P. Nuij and M. Steinbuch, Two measurement techniques to determine higher order sinusoidal input describing functions, Proceedings of ISMA 2004, Leuven, Belgium, (2004) 2145-2154.

[2] P. Dahl, A solid friction model, Aerospace Corp., El Segundo, CA, Tech. Rep. TOR-0158 (3107-18)-1 (1968).

[3] C. Canudas de Wit, H. Olsson, K. J. Åström and P. Lischinsky, A new model for control of systems with friction, *IEEE Transactions on Automatic Control* 40 (3) (1995) 419-425.

[4] J. Swevers, F. Al-Bender, C. G. Ganseman and T. Prajogo, An integrated friction model structure with

improved presliding behavior for accurate friction compensation, *IEEE Transactions on Automatic Control* 45 (4) (2000) 675-686.

[5] P. Dupont, V. Hayward, B. Armstrong and F. Altpeter, Single state elastoplastic friction models, *IEEE Transactions on Automatic Control* 47 (5) (2000) 787-792.

[6] C. Hsieh and Y. -C. Pan, Dynamic behavior and modeling of the pre-sliding static friction, *Wear* 242 (2000) 1-17.

[7] V. Lampaert, J. Swevers and F. Al-bender, Modification of the Leuven integrated friction model structure, *IEEE Transactions on Automatic Control* 47 (4) (2002) 683-687S.

[8] R. H. A. Hensen, M. J. G. van de Molengraft and M. Steinbuch, Frequency domain identification of dynamic friction model parameters, *Transactions on Control Systems Technology* 10 (2) (2002) 191-196.

[9] T. -Y. Lin, Y. -C. Pan, and C. Hsieh, Precision-limit positioning of direct drive systems with the existence friction, *Control Engineering Practice* 11 (2003) 233-244.

[10] J. -S. Chen, K. -C. Chen, Z. -C. Lai and Y. -K. Huang, Friction characterization and compensation of a linear-motor rolling-guide stage, *International Journal of Machine Tools & Manufacture* 43 (2003) 905-915.

[11] H. Ohta, Sound of linear guideway type recirculating linear ball bearings, *Transactions of the ASME, Journal of Tribology* 121 (1999) 678-685.

[12] H. Ohta and E. Hayashi, Vibration of linear guideway type recirculating linear ball bearings, *Journal of Sound and Vibration* 235 (5) (2000) 847-861.

[13] S. Mekid, High precision linear slide. Part I: design and construction, *International Journal of Machine Tools & Manufacture* 40 (2000) 1039-1050.

[14] Futami, A. Furutani, and S. Yoshida, Nanometer positioning and its micro-dynamics, *Nanotechnology* 1 (1990) 31-37.

[15] J. Otsuka and T. Masuda, The influence of nonlinear spring behavior of rolling elements on ultraprecision positioning control systems, *Nanotechnology* 9 (1998) 85-92.

[16] S. Shimizu, E. Saito and H. Uchida, Tribological studies of linear motion ball guide systems, *Tribology Transactions* 41 (1) (1998) 49-59.

[17] K. L. Johnson, Contact Mechanics, Cambridge University Press, Cambridge, UK, (1985).

[18] J. S. Choi, J. Yoo, Y. -S. Yi, Y. Y. Kim, D. J. Lee and S. J. Lee, Vibration analysis and its application of a linear motion guide supported by rolling ball bearings, *Transactions of KSME A* 29 (7) (2005) 955-963.

[19] C. Canudas de Wit and P. Lischinsky, Adaptive friction compensation with partially known dynamic friction model, *International Journal of Adaptive Control and Signal Processing* 11 (1997) 65-80.

Appendix

If the mass of the bearing ball is so small that it cannot affect the system behavior, the total contact system can be easily expressed as a one degree-of-freedom oscillator. From Eq. (7), the new relationship between the contact load P and the displacement q can be derived as

$$P = \frac{C}{2\sqrt{2}} q^{3/2},\ C = \frac{0.60E^{*}\pi\left(R'R''\right)^{\frac{1}{4}}}{\sqrt{2}},\ q = 2\delta \quad \text{(A1)}$$

Then the linear spring stiffness k can be obtained by differentiating Eq. (A1) for q.

If the LM block moves in the vertical direction by dz, the spring of the upper surface is elongated by dz and that of lower surface shrinks by $dz \sin\beta$ as shown in Fig. A1. The LM system is symmetric about the vertical direction, so the motion of equation in the vertical direction can be derived as follows.

$$M\ddot{z} = 2C_{eq}\left(z_1 - dz\right)^{3/2} - 2C_{eq}\sin\beta\left(z_2 + dz\sin\beta\right)^{3/2} \quad \text{(A2)}$$

where C_{eq} is a constant which multiplies $\frac{C}{2\sqrt{2}}$ by the number of balls in one row, and z_1 denotes the initial displacement of bearing balls of the upper rows

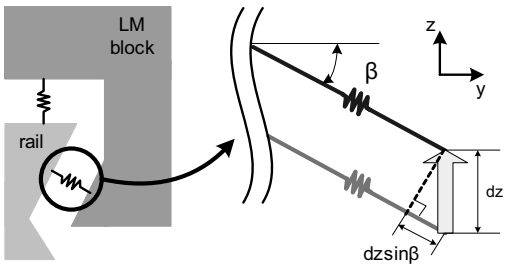

Fig. A1. Relationship between the displacement of the upper row and the lower row.

caused by the minus tolerance and z_2 the initial displacement of lower rows. If the system is assumed to reach static equilibrium at $dz = 0$, the following relation between the initial displacement of balls in the upper and lower rows can be obtained:

$$\left(\frac{z_1}{z_2}\right)^{3/2} = \sin\beta \tag{A3}$$

For simpler analysis, the arrays of the balls can be assumed to be continuous. Then, the spring constant *K* per unit length can be written as

$$K = \frac{Nk}{L} \tag{A4}$$

where *N* and *L* represent the average number of balls in the load zone and the length of load zone on the circuit of the recirculating balls, respectively.

Using the notation used in section 3.2, the kinetic energy of the 5 degree-of-freedom system becomes

$$T = \frac{1}{2}M\dot{y}^2 + \frac{1}{2}M\dot{z}^2 + \frac{1}{2}J_x\dot{\phi}^2 + \frac{1}{2}J_y\dot{\theta}^2 + \frac{1}{2}J_z\dot{\psi}^2 \tag{A5}$$

The potential energy by the elastic deformation of the ball bearings can be formulated as the integration for loading length.

$$\begin{aligned} U = \frac{1}{2}\int_{-L/2}^{L/2}\Big[& K_1\{(y + a\phi + l\psi)\cos\alpha + (z + c_1\phi - l\theta)\sin\alpha\}^2 \\ & + K_2\{(y + b\phi + l\psi)\cos\beta - (z + c_2\phi - l\theta)\sin\beta\}^2 \\ & + K_2\{-(y + b\phi + l\psi)\cos\beta - (z - c_2\phi - l\theta)\sin\beta\}^2 \\ & + K_1\{-(y + a\phi + l\psi)\cos\alpha + (z - c_1\phi - l\theta)\sin\alpha\}^2\Big]dl \end{aligned} \tag{A6}$$

where K_1 denotes the equivalent stiffness of the upper rows and K_2 the stiffness of the lower rows.

Using T and U, the following five equations of motion can be derived from the Euler-Lagrange equations:

$$M\ddot{y} + (2K_1L\cos^2\beta)y + K_2L(2b\cos^2\beta - c_2\sin 2\beta)\phi = 0 \tag{A7}$$

$$M\ddot{z} + 2L(K_1 + K_2\sin^2\beta)z = 0 \tag{A8}$$

$$\begin{aligned} & J_x\ddot{\phi} + 2L(K_1c_1^2 + K_2b^2\cos^2\beta + K_2c_2^2\sin^2\beta - K_2bc_2\sin 2\beta)\phi \\ & + L(2K_2b\cos^2\beta - K_2c_2\sin 2\beta)y = 0 \end{aligned} \tag{A9}$$

$$J_y\ddot{\theta} + \frac{KL^3}{6}(1 + \sin^2\beta)\theta = 0 \tag{A10}$$

$$J_z\ddot{\psi} + \left(\frac{KL^3}{6}\cos^2\beta\right)\psi = 0 \tag{A11}$$

Eqs. (A7)-(A11) represent the equations of motion or high-order rolling, bouncing, rolling, pitching and yawing mode, respectively. From Eqs. (A8), (A10) and (A11), the natural frequencies are easily obtained because z, θ and ψ are uncoupled.

$$f_{bouncing} = \frac{1}{2\pi}\sqrt{\frac{2L(K_1 + K_2\sin^2\beta)}{M}} \tag{A12}$$

$$f_{pitching} = \frac{1}{2\pi}\sqrt{\frac{L^3(K_1 + K_2\sin^2\beta)}{6J_y}} \tag{A13}$$

$$f_{yawing} = \frac{1}{2\pi}\sqrt{\frac{K_2L^3\cos^2\beta}{6J_Z}} \tag{A14}$$

Because y and ϕ are coupled, the natural frequencies for rolling and high order-rolling modes can be obtained by solving the following equations:

$$\begin{aligned} & y = Ye^{j\omega t},\ \phi = \Phi e^{j\omega t} \\ & \begin{bmatrix} p_1 - M\omega^2 & p_2 \\ p_2 & p_3 - J_x\omega^2 \end{bmatrix}\begin{Bmatrix} Y \\ \Phi \end{Bmatrix} = \begin{Bmatrix} 0 \\ 0 \end{Bmatrix} \end{aligned} \tag{A15}$$

where

$$\begin{aligned} p_1 &= 2K_2L\cos^2\beta \\ p_2 &= K_2L(2b\cos^2\beta - c_2\sin 2\beta) \\ p_3 &= 2L(K_1c_1^2 + K_2b^2\cos^2\beta + K_2c_2^2\sin^2\beta - K_2bc_2\sin 2\beta) \end{aligned} \tag{A16}$$

To obtain a non-trivial solution, the determinant of the square matrix in Eq. (A15) must be zero. The results are

$$\begin{cases} f_{rolling} = \omega_1/2\pi \\ f_{high-rolling} = \omega_2/2\pi \end{cases} \tag{A17}$$